

Optimized Intermolecular Potential for Aromatic Hydrocarbons Based on Anisotropic United Atoms. 2. Alkylbenzenes and Styrene

R. Oliver Contreras-Camacho,^{†,‡} Philippe Ungerer,^{§,||} M. Goktug Ahunbay,[§] Véronique Lachet,^{||} Javier Perez-Pellitero,[†] and Allan D. Mackie^{*,†}

Departament d'Enginyeria Química, ETSEQ, Universitat Rovira i Virgili, Avinguda dels Països Catalans 26, Campus Sescelades, 43007 Tarragona, Spain, Laboratoire de Chimie Physique, Université de Paris Sud, Bâtiment 349, 91405 Orsay Cedex, France, and Institut Français du Pétrole, 1-4 Avenue de Bois Préau, 92852 Reuil-Malmaison, Cedex, France

Received: March 24, 2004; In Final Form: June 28, 2004

An optimization has been performed for the parameters of an Anisotropic United Atoms (AUA) intermolecular potential for thermodynamic property prediction using both Gibbs ensemble and NPT Monte Carlo simulations. The model uses the same parameters as previous AUA models for the aromatic CH, alkyl CH₂, and methyl CH₃ groups as well as the CH and CH₂ groups for olefins. The optimization procedure is based on the minimization of a dimensionless error criterion incorporating various thermodynamic data of *p*-xylene at 311 and 491 K. The model has been evaluated on a series of alkylbenzenes and styrene including toluene, *o*- and *m*-xylene, trimethylbenzene, *n*-propylbenzene, *n*-hexylbenzene, and *n*-dodecylbenzene from ambient temperature to near-critical temperature. Vaporization enthalpy, liquid density, and normal boiling temperature are reproduced with an average error of 2% or lower. Although the proposed AUA model is very simple, as it does not include any electrostatic charges, it accounts fairly well for the influence of the alkyl substituents over a large range of temperature and carbon number.

1. Introduction

Following the development of the Gibbs ensemble method, which allows for the efficient determination of the liquid–vapor equilibrium properties by Monte Carlo simulation,¹ several types of intermolecular potentials have been proposed to provide quantitative predictions for hydrocarbons. The most frequent type of potential is based on the concept of the United Atom (UA), in which the carbon and its bonded hydrogens are represented by a single Lennard–Jones force center, the interaction site being located at the carbon nucleus. Several UA parametrizations have been proposed for *n*-alkanes,^{2–5} branched alkanes,^{6,7} α -olefins,^{8–10} and alkylbenzenes.⁹ This type of model provides good results, but the search for more quantitative calculations has triggered the investigation of alternative models.

A first alternative to classical UA consists of using another type of repulsion energy function, namely, the exponential-6 potential. This was developed for *n*-alkanes,¹¹ benzene, and cyclohexane.¹² A second alternative consists of using explicit hydrogens instead of UA.¹³ Both strategies provide significant improvements on the families investigated. However, they are not applicable to a large range of hydrocarbon families from the literature published so far. The third alternative consists of using Anisotropic United Atoms (AUA) (i.e., united atoms in which the Lennard–Jones interaction site is offset from the carbon nucleus to be shifted toward the hydrogen atoms). This potential has been developed for *n*-alkanes,¹⁴ branched alkanes,¹⁵ cyclic alkanes,¹⁶ and olefins.¹⁷ Although its development has required a small number of parameters, the AUA potential has

been shown to provide predictions over a large range of carbon number and temperature. This may be attributed to the physical sense of its parameters, as the offset of the Lennard–Jones sphere allows for a better account of the hydrogens than in the classical UA approach.

The development of AUA-type potentials for aromatic hydrocarbons has already been explored in a recent work by Friedrich and Lustig dedicated to benzene.¹⁸ In the first paper of the present series, we have proposed a new parametrization of the CH aromatic group parameters with the AUA model on the basis of vapor–liquid equilibrium properties at 293 and 450 K.¹⁹ We showed that the new AUA parameters do not exhibit major differences with Friedrich and Lustig's model. Both AUA parametrizations provide significant improvements as compared with classical UA potentials of benzene since they better reproduce the vaporization enthalpy and the carbon–carbon radial distribution function of liquid benzene.

The purpose of the present article is to extend the AUA potential to alkylbenzenes, without reconsidering the parametrization of the CH aromatic,¹⁹ the CH₂ and CH₃ groups of alkanes,¹⁴ nor the CH and CH₂ groups for olefins. For this purpose, we use *p*-xylene as a reference alkylbenzene to calibrate the parameters of the aromatic carbon on which the alkyl substituents are attached. The model is then tested on alkylbenzenes that were not used to optimize the potential parameters.

The paper is organized as follows. In the first section, we present the simulation algorithms and give the expressions used for the intermolecular and the intramolecular potential energy. In the second section, we detail the procedure followed to obtain the parameters of the new aromatic carbon group. The third section is devoted to the evaluation of the model on seven alkylbenzenes from 7 to 18 carbon atoms and styrene. In the fourth section, we discuss the results obtained with the new AUA potential.

* Corresponding author e-mail: amackie@etseq.urv.es.

[†] Universitat Rovira i Virgili.

[‡] Presently at Institut Français du Pétrole.

[§] Université de Paris Sud.

^{||} Institut Français du Pétrole.

2. Simulation Method

2.1. Potential Energy and Structural Models. Following the choice made in the previous AUA models of hydrocarbons,^{14,15,19} the effective intermolecular dispersion–repulsion interactions between two atoms or united atoms (*i* and *j*) are represented by the Lennard–Jones 6-12 equation, using the Lorentz–Berthelot combining rules to compute cross-coefficients.

The intramolecular interactions are computed by a summation of bending energy, torsional energy, and distant neighbor interaction energy. No stretching energy is considered as the bond lengths are considered to be constant. The expressions for the bending potential energy:

$$U^{\text{bend}}/k = \frac{1}{2}k_{\text{bend}}(\cos \theta - \cos \theta_0)^2 \quad (1)$$

and for the torsion potential energy:

$$U^{\text{tors}}/k = \sum_{j=0}^8 a_j (\cos \phi)^j \quad (2)$$

are identical to those of Toxvaerd,²⁰ where *k* is the Boltzmann constant, θ is the bond angle, and ϕ is the dihedral angle (with the convention that $\phi = 0$ for the trans configuration). The distant neighbor energy between groups separated by more than three bonds is computed with the same AUA potential as for intermolecular interactions.

The aromatic cycle is considered to be rigid with hexagonal symmetry, a very common assumption in molecular models.^{12,18,21,22} In an alkyl substituent on a ring, the carbon in the α position is considered to lie in the aromatic ring plane with 120° bond angles, another common assumption.^{9,23} As a consequence, the bending and torsion potentials considered in alkylbenzenes are those involving at least two saturated carbons.

2.2. Statistical Ensembles and Monte Carlo Algorithms. Periodic boundary conditions are implemented with the minimum image convention.²⁴ Dispersion and repulsion interactions were evaluated with a spherical cutoff radius equal to half of the simulation box length, associated with standard long-range corrections.

2.2.1. Gibbs Ensemble Simulations. The Gibbs ensemble Monte Carlo method¹ is used to compute phase equilibria. The Monte Carlo moves implemented are translations, rigid body rotations, flips,^{15,25} configurational bias regrowth and transfers,² and volume changes. For rigid molecules, we use also a two-step statistical bias involving the selection of a suitable location for the center of mass in a first step and the test of several orientations in a second step.¹⁶ The selected probabilities for rigid molecules are generally 0.3 for translations and rotations, 0.395 for transfers, and 0.005 for volume changes. In the case of flexible molecules, typical probabilities are 0.15 for translations, rigid body rotations, flip, and regrowth; 0.395 for transfers; and 0.005 for volume changes. The simulations are carried out using a total of 150–256 molecules with at least 1400 force centers.

The molar vaporization enthalpy is computed as the difference between the average molar enthalpies of the liquid and of the vapor simulation boxes. The statistical uncertainty on this property is typically 1–2%. The average liquid density is generally determined with statistical uncertainty of 0.5–1%, but higher values (up to 5%) are found at near-critical temperatures as a result of the larger fluctuations. Once we have computed the vapor–liquid coexistence density curves, the critical tem-

perature is obtained by fitting the critical scaling law $\rho_l - \rho_v = \lambda(T_c - T)^{0.325}$. The law of rectilinear diameters, $1/2(\rho_l + \rho_v) = \rho_c + \gamma(T - T_c)$, is then used to estimate the critical density.

2.2.2. Equilibrium Properties below the Normal Boiling Point. To circumvent the poor acceptance ratio of Gibbs ensemble simulations below the normal boiling temperature, simulations in the NpT isothermal–isobaric ensemble are performed to obtain the saturated liquid properties. The molar enthalpy of vaporization is given by the following equation:

$$\Delta H_{\text{vap}} = -\langle E_{\text{liq}(\{\text{int}\}_{\text{er}})} \rangle + RT \quad (3)$$

where $\langle E_{\text{liq}(\{\text{int}\}_{\text{er}})} \rangle$ is the average molar intermolecular potential energy in the simulation. This relationship assumes that (i) the molar volume of the liquid is negligible compared with the vapor and (ii) the vapor is close enough to that of an ideal gas. These assumptions are correct below the normal boiling point because of the low density of the saturated vapor. As liquid properties are not significantly different when pressure is set to the true vapor pressure or to zero, the NpT simulations are made at zero pressure.

To determine the saturated vapor pressures, the NpT simulations were made at constant intervals in a $1/T$ scale to use the thermodynamic integration of the Clapeyron equation²⁶ with a second-order numerical integration algorithm.¹⁴ This yields the following working equation:

$$\ln(P^{\text{sat}}(T_{n+2k})) = \ln(P^{\text{sat}}(T_n)) - \frac{2}{R} \Delta(1/T) \sum_{i=1}^k \Delta H_{\text{vap}}(T_{n+2i-1}) \quad (4)$$

where $\Delta(1/T) = 1/T_i - 1/T_{i+1}$ is the constant spacing of the temperatures on the inverse temperature scale, T_n being a temperature where a Gibbs ensemble simulation has been performed.

An important aspect in thermodynamic integration is the estimation of statistical uncertainties. In the summation of the right-hand side of eq 4, we have observed that for a given compound, the statistical uncertainties are equivalent at the different temperatures. We may then apply the square root dependence of the standard deviation versus the number of independent variables in the sum:

$$\sigma\left(\sum_{i=1}^k \Delta H_{\text{vap}}(T_{n+2i-1})\right) \approx \sqrt{k} \sigma(\Delta H_{\text{vap}}) \quad (5)$$

A conservative way to evaluate the standard deviation on $\ln(P^{\text{sat}}(T_{n+2k}))$ is then to sum the standard deviations on $\ln(P^{\text{sat}}(T_n))$ and on the summation term:

$$\sigma(\ln(P^{\text{sat}}(T_{n+2k}))) \approx \sigma(\ln(P^{\text{sat}}(T_n))) + \frac{2\sqrt{k}}{R} \Delta(1/T) \sigma(\Delta H_{\text{vap}}) \quad (6)$$

The standard logarithmic deviation on $\ln(P^{\text{sat}})$ appears thus as the sum of the contributions of the starting point and of the integration process. The contribution of thermodynamic integration does not increase as the number of integration steps but as its square root. For a typical case of a vapor pressure calculation at low temperature like *n*-propylbenzene, the standard logarithmic deviation due to the Gibbs ensemble starting point is 0.03 and the standard deviation on vaporization enthalpy is 0.1 kJ/mol. If the number *k* is 4 (half the total number of integration steps) and $\Delta(1/T) = 2.10^{-4} \text{ K}^{-1}$, the contribution of thermodynamic integration to the standard logarithmic deviation is

TABLE 1: Location of Force Centers and Lennard–Jones Parameters of the AUA Intermolecular Potential of Aromatic Hydrocarbons

ref	group	σ (Å)	ϵ/k (K)	B (Å) ^a	δ (Å) ^b
this work	C	3.0648	42.079	1.40	0
19	CH	3.2464	89.415	1.8071	0.4071
14	CH ₂	3.4612	86.29		0.384
	CH ₃	3.6072	120.15		0.216
17	CH (π -bonded)	3.32	90.6		0.414
	CH ₂ (π -bonded)	3.48	111.1		0.295

^a Distance between the center of the molecule and the interaction site. ^b Offset distance between the carbon center and the interaction site.

approximately 0.01 (i.e., much lower than the contribution from the Gibbs ensemble starting point). The statistical uncertainties given in the tables are given at the 99% confidence level (i.e., they are estimated as 2.5 times the standard deviations).

2.3. Optimization Method of Force Field Parameters. The following dimensionless error criterion is used:¹⁴

$$F = \sum_{i=1}^n \frac{(X_i^{\text{mod}} - X_i^{\text{exp}})^2}{s_i^2} \quad (7)$$

where X_i^{exp} is the reference experimental measurements [either $\ln(P^{\text{sat}})$, ΔH_{vap} , ρ_l], X_i^{mod} is the associated computed properties, and s_i is the estimated statistical uncertainty on X_i^{mod} estimated by the standard block averaging technique.²⁴ F is considered to be a function of the parameters y_j to be optimized. The minimization of F with respect to all y_j is made by approximating the function by its first-order Taylor expansion. For this purpose, the partial derivatives $\partial X_i^{\text{mod}} / \partial y_k$ are evaluated by finite differences with the initial set of parameters.

3. Determination of Potential Parameters

Our purpose is to keep unchanged the Lennard–Jones parameters of the aromatic CH group¹⁹ as well as the CH₂ and CH₃ alkyl groups¹⁴ and the CH and CH₂ olefinic groups,¹⁷ which are given in Table 1.

We decided, for all methyl aromatics, to fix the bond distance between the aromatic carbon and the sp³ carbon to the same value as the bond distance between two sp³ carbons in the OPLS representation²³ (i.e., 1.51 Å). This bond distance is indeed very close in toluene, where it is 1.524 Å.²⁷ Otherwise, the bond distance between aromatic carbon and the sp³ carbon of an alkyl chain is fixed to 1.535 Å, the same bond distance between two sp³ carbons in the previous AUA potentials considering linear chains.¹⁴ The bond length between aromatic carbons has been set to 1.40 Å, as in our study of benzene.¹⁹

The bending potential parameters in the alkyl chain have been selected to be identical to the AUA potential of *n*-alkanes (i.e., $k_{\text{bend}} = 74900$ K and $\theta_0 = 114^\circ$) for all flexible bond angles in the alkyl chain, including the first angle involving an aromatic carbon and the first two sp³ carbons of the chain.

The torsion potential was also taken to be identical to the *n*-alkane AUA model²⁰ for all dihedral angles involving three or four sp³ carbons. The torsional energy associated with the dihedral angle involving two aromatic carbons and the first two sp³ carbons of a chain was described by the same set of parameters as for olefins.²⁸ The torsion parameters are shown in Table 2.

The parameters of the aromatic carbon bonded to the alkyl substituent have been determined as follows. The interaction

TABLE 2: Torsion Parameters of the AUA Potential of Alkylbenzenes

sequence	parameters (K)
C—CH ₂ —CH ₂ —C (alkyl chains)	$a_0 = 1001.35$, $a_1 = 2129.52$, $a_2 = -303.06$, $a_3 = -3612.27$, $a_4 = 2226.71$, $a_5 =$ 1965.93 , $a_6 = -4489.34$, $a_7 =$ -1736.22 , $a_8 = 2817.37$
C=CH—CH ₂ —C (alkylaromatics)	$a_0 = 272.37$, $a_1 = -938.12$, $a_2 = 220.73$, $a_3 = 1135.06$, $a_4 = 0$
C=C=C=C (aromatics)	$\phi = 180^\circ$ (planar cycle)
C=C=C—X (first substituent)	$\phi = 0^\circ$ (first alkyl carbon is in aromatic plane)

TABLE 3: Reference Data and Simulation Conditions Used for Optimization of Parameters of Aromatic C Group on *p*-Xylene Properties^a

T (K)	simulation conditions	type of data	AUA-Arom (this work)	exptl data
491	GEMC	P^{sat} (kPa) (kJ/mol) ρ_l (kg/m ³)	740.0 28.8 665.39	576.2 29.8 665.04
311	monophasic, NpT, $P = 0$	ΔH_{vap} (kJ/mol) ρ_l (kg/m ³)	41.4 862.7	41.5 845.8

^a Vapor pressure (P^{sat}), vaporization enthalpies (ΔH_{vap}), and liquid densities (ρ_l).

site was placed on the carbon nucleus for symmetry reasons. There are thus only the two parameters (ϵ and σ) of the Lennard–Jones potential to determine. For this purpose, we used the optimization method outlined in section 2.3. It is expected that the optimization of such a branched carbon is delicate because it cannot be in contact with more than two sites of neighboring molecules, so that its influence on thermodynamic properties is low as compared to the adjacent aromatic or methyl groups. The reference properties defining the error criterion were thus taken from *p*-xylene since this molecule contains two force centers of the type considered. We considered equilibrium properties in two reference states at 311 and 491 K, which were simulated in the NpT ensemble and the Gibbs ensemble. In both states, the liquid density and the molar vaporization enthalpy were introduced in the criterion, but the saturation pressure could be taken into account at 491 K only. The initial parameters were $\sigma = 3.0147$ Å and $\epsilon/k = 68.431$ K. The parameters arising from the optimization are given in Table 1 (i.e., $\sigma = 3.065$ Å and $\epsilon/k = 42.08$ K for the aromatic C group). A comparison of simulated and reference properties is shown in Table 3. The vaporization enthalpy and the liquid density are well predicted, while the saturation pressure is significantly overpredicted. It was nevertheless decided to evaluate the model because saturation pressure varies very fast with temperature, so that the error on the normal boiling point may be expected to stay within acceptable limits.

4. Evaluation of the Optimized AUA Model

The proposed potential has been tested on various alkylbenzenes other than the *p*-xylene, which served to optimize the AUA parameters of the new aromatic carbon group: styrene, toluene, *o*-xylene, *m*-xylene, 1,3,5-trimethylbenzene, *n*-propylbenzene, *n*-hexylbenzene, and *n*-dodecylbenzene. This evaluation was complemented by the determination of *p*-xylene properties at other temperatures than those used in the optimization.

The aromatics comprising methyl or vinyl substituents are grouped in Tables 4 and 5. Toluene, 1,3,5-trimethylbenzene, and styrene have been investigated by Gibbs ensemble simulations at several temperatures above the normal boiling temper-

TABLE 4: Comparison of Predicted and Experimental Equilibrium Properties of Toluene, 1,3,5-Trimethylbenzene, and Styrene^a

<i>T</i> (K)	ensemble	property	calcd values	exptl values	% dev
Toluene					
301	NpT	ΔH_{vap}	37.7 ₂	37.9	−0.5
		ρ_l	866.5 _{0.5}	861.3	0.6
405	Gibbs	P^{sat}	221 ₁₇	179	23.5
		ΔH_{vap}	31.7 ₃	32.1	−1.2
		ρ_l	758.9 _{1.1}	757.3	0.2
471	Gibbs	P^{sat}	891 ₂₁	724	23.1
		ΔH_{vap}	26.6 ₃	27.3	−2.6
		ρ_l	675.9 _{0.7}	677.4	−0.2
527	Gibbs	P^{sat}	2215 ₆₁	1773	24.9
		ΔH_{vap}	19.8 ₂	21.7	−8.8
		ρ_l	579.5 ₅	591.0	−1.9
1,3,5-Trimethylbenzene					
350	NpT	ΔH_{vap}	40.6 ₁	44.7	−9.2
		ρ_l	837.8 _{1.1}	819.1	2.3
450	Gibbs	P^{sat}	200.0 ₁₈	139.45	43.4
		ΔH_{vap}	36.6 ₂	38.4	−4.7
		ρ_l	735.4 _{2.2}	724.9	1.4
471	Gibbs	P^{sat}	326 ₂₉	226	44.2
		ΔH_{vap}	34.5 ₂	36.7	−6.0
		ρ_l	706.5 _{2.4}	702.5	0.6
525	Gibbs	P^{sat}	872 ₁₀	644	35.4
		ΔH_{vap}	28.8 ₃	31.9	−9.7
		ρ_l	633.6 _{6.8}	637.7	−0.6
530	Gibbs	P^{sat}	941.2 ₄₄	701.7	34.1
		ΔH_{vap}	28.3 ₃	31.5	−10.2
		ρ_l	628.5 _{1.3}	631.0	−0.4
Styrene					
360	Gibbs	P^{sat}	21.4 _{0.8}	15.94	34.3
		ΔH_{vap}	40.7	40.8	−0.2
		ρ_l	843.3 _{1.8}	843	0.0
383	Gibbs	P^{sat}	31.9 _{0.6}	35.8	−10.9
		ΔH_{vap}	39.3	39.4	−0.3
		ρ_l	821.6 _{1.6}	820.7	0.1
418	Gibbs	P^{sat}	120 ₅	99.7	20.4
		ΔH_{vap}	36.7	37.1	−1.1
		ρ_l	783.2 _{1.5}	784.8	−0.2
500	Gibbs	P^{sat}	676.6 ₂₀	575	17.7
		ΔH_{vap}	30.4	30.6	−0.7
		ρ_l	689.7 ₂	689.8	0.0
540	Gibbs	P^{sat}	1345.4 ₁₉	1096	22.8
		ΔH_{vap}	26.2	26.6	−1.5
		ρ_l	632.9 _{2.2}	634.1	−0.2
580	Gibbs	P^{sat}	2369 ₃₃	1921	23.3
		ΔH_{vap}	23.4	21.4	9.3
		ρ_l	554.2 _{3.8}	565.7	−2.0

^a Vapor pressure (P^{sat}) is expressed in kPa, vaporization enthalpies (ΔH_{vap}) is in kJ/mol, and liquid density (ρ_l) is in kg/m³.

ature. A complementary NpT simulation was performed at a temperature close to ambient (301 K for toluene and 350 K for trimethylbenzene). The liquid density, vaporization enthalpy, and saturated vapor pressures of these three hydrocarbons are given in Table 4 and Figures 1–3. It can be seen that the liquid density and the vaporization enthalpy at low temperature (301 or 311 K) are well reproduced, as the maximum deviation is less than 2.6% for toluene and styrene at these conditions (Table 4). Figure 1 illustrates the good agreement of the vaporization enthalpy with experimental information but also shows a tendency to underestimate the critical temperature in a systematic way since vaporization enthalpy decreases too fast when approaching the critical temperature. At higher temperatures, the vaporization enthalpy seems indeed to be underestimated (Figure 1). 1,3,5-Trimethylbenzene shows the largest deviations on comparing the vaporization enthalpy, and a maximum deviation of 10% is found for this property at 530 K. However,

TABLE 5: Comparison of Predicted and Experimental Equilibrium Properties of *o*-Xylene, *m*-Xylene, and *p*-Xylene^a

<i>T</i> (K)	ensemble	property	calcd values	exptl values	% dev
<i>o</i> -Xylene					
311	NpT	ΔH_{vap}	41.8 ₁	42.8	−2.3
		ρ_l	874.5 _{1.07}	865.4	1.1
333	NpT	ΔH_{vap}	39.2 ₂	41.7	−6.0
		ρ_l	853.9 _{1.8}	846.9	0.8
400	Gibbs	P^{sat}	93.5 ₁₂	62.4	49.8
		ΔH_{vap}	36.5 ₂	37.7	−3.2
		ρ_l	788.2 _{1.6}	786.7	0.2
491	Gibbs	P^{sat}	723 ₁₁	510	41.8
		ΔH_{vap}	29.4 ₃	31.3	−6.1
		ρ_l	679.4 _{1.6}	690.2	−1.6
577	Gibbs	P^{sat}	2493 ₂₄	1937	28.7
		ΔH_{vap}	17.7 ₃	21.7	−18.4
		ρ_l	511.8 _{1.8}	562.1	−8.9
<i>m</i> -Xylene					
360	Gibbs	P^{sat}	26.2 ₁	19.6	33.7
		ΔH_{vap}	38.3	39.4	−2.8
		ρ_l	810.6 _{1.1}	806.5	0.5
420	Gibbs	P^{sat}	170.8 ₈	124.2	37.5
		ΔH_{vap}	34.6	35.7	−3.1
		ρ_l	754.5	0.8748.6	0.8
459	Gibbs	P^{sat}	453.3 ₂₆	307	47.7
		ΔH_{vap}	31.4	32.9	−4.6
		ρ_l	709.8 _{1.8}	706.6	0.5
512	Gibbs	P^{sat}	1050.6 ₂₃	823	27.7
		ΔH_{vap}	26.4	28.2	−6.4
		ρ_l	633.3 _{2.1}	640.5	−1.1
550	Gibbs	P^{sat}	1870 ₁₄	1479	26.8
		ΔH_{vap}	22.9	23.9	−4.2
		ρ_l	563.9 _{2.4}	582	−3.1
<i>p</i> -Xylene					
311	NpT	ΔH_{vap}	41.4 ₂	41.5	−0.2
		ρ_l	862.7 _{0.9}	845.8	2.0
374	Gibbs	P^{sat}	44 ₂	33.0	33.3
		ΔH_{vap}	37.8 ₂	38.2	−1.0
		ρ_l	802.9 _{0.4}	789.6	1.7
491	Gibbs	P^{sat}	740 ₅₂	576	28.5
		ΔH_{vap}	28.8 ₂	29.8	−3.4
		ρ_l	665.4 _{1.5}	665.0	0.1
522	Gibbs	P^{sat}	1248 ₅₂	972	28.4
		ΔH_{vap}	25.0 ₃	27.0	−7.4
		ρ_l	614.5 _{2.7}	621.3	−1.1

^a Vapor pressure (P^{sat}) is expressed in kPa, vaporization enthalpies (ΔH_{vap}) is in kJ/mol, and liquid density (ρ_l) is in kg/m³.

it should be pointed out that this point (see Figure 2) is close to the critical temperature where large fluctuations in density produces large uncertainties in properties. The liquid density is very well reproduced over the whole temperature range for all three hydrocarbons (Table 4 and Figure 2). The vapor pressure is generally overestimated for the three hydrocarbons tested in Table 4, confirming the tendency noticed for *p*-xylene when optimizing the potential parameters (Figure 6).

The xylene isomers (*o*-, *m*-, and *p*-xylene) have also been studied. Simulation results are summarized in Table 5 and in Figures 4–6. An underestimation in vaporization enthalpy of about 3% at temperatures far from critical conditions has been found. Once again, the vapor pressure is overestimated for the three isomers. Nevertheless, a very good agreement is obtained when comparing experimental and simulated saturation liquid densities. A maximum deviation of less than 1.6% is obtained in the liquid density (Table 5) with the exception of the 577 K point of *o*-xylene. As shown in Figure 5, this point is close to critical conditions, where density varies very fast, which may explain such an important deviation. Some small systematic differences are found between the isomers such as the higher

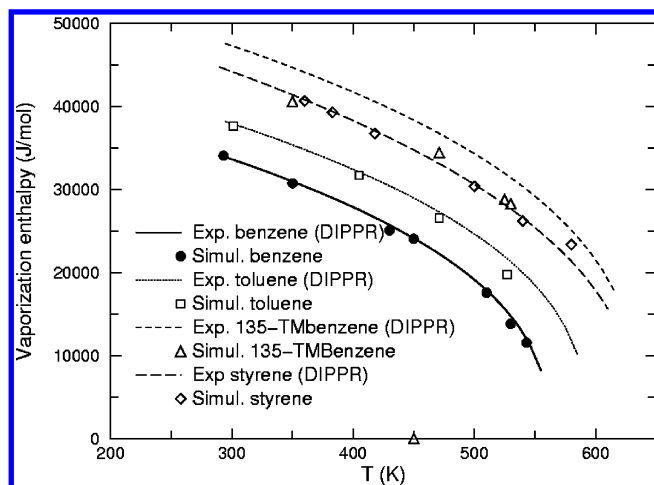


Figure 1. Vaporization enthalpy of benzene,¹⁹ toluene, 1,3,5-trimethylbenzene, and styrene computed with the new AUA potential. Comparison is given with the correlations of experimental data provided by the Dortmund Data Bank.

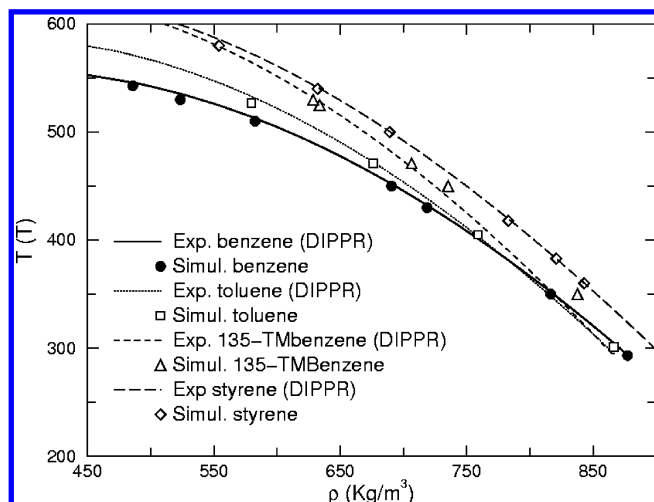


Figure 2. Saturated liquid density of benzene,¹⁹ toluene, 1,3,5-trimethylbenzene, and styrene computed with the new AUA potential. Comparison is given with the correlations of experimental data provided by the Dortmund Data Bank.

liquid density and higher vaporization enthalpy of *o*-xylene. However, it is clear that the proposed model does not satisfactorily account for the observed differences between the various xylenes.

The *n*-propylbenzene molecule has been simulated above the normal boiling point at four temperatures in the Gibbs ensemble, ranging from 450 to 600 K. Five temperatures, regularly spaced on the $1/T$ scale, have been simulated with the NpT ensemble to obtain vapor pressures by thermodynamic integration down to 300 K (Table 6). The *n*-hexylbenzene molecule has been simulated at three temperatures in the Gibbs ensemble (494–616 K) and six temperatures in the NpT ensemble, down to 310 K (Table 7). In this table, a comparison is given with the pseudo-experimental correlation available from the Dortmund Data Bank. Consistency with recent measurements of vapor pressures has been checked.²⁹ The *n*-dodecylbenzene molecule has been simulated at 611 and 700 K in the Gibbs ensemble and at eight temperatures in the NpT ensemble, down to 298 K (Table 8). The general behavior of these three *n*-alkylbenzenes is very similar to the methyl-substituted aromatics of Table 4: the vaporization enthalpy and the liquid density are very well reproduced over the whole range of temperature investigated (Figures 7 and 8). Figure 9 shows that the errors noticed for

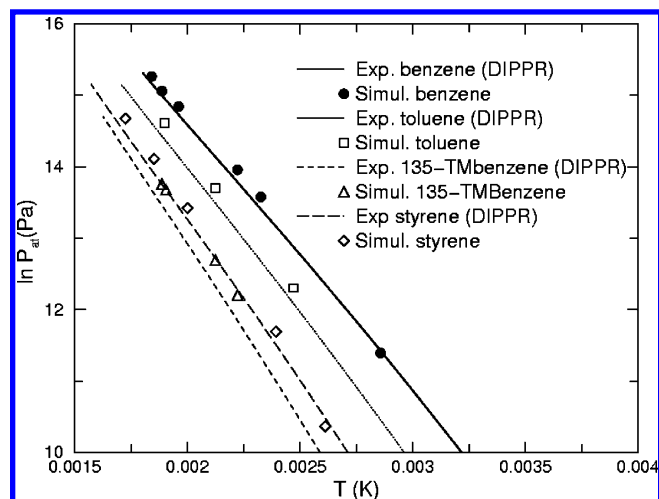


Figure 3. Vapor pressures of benzene,¹⁹ toluene, 1,3,5-trimethylbenzene, and styrene computed with the new AUA potential. Comparison is given with the correlations of experimental data provided by the Dortmund Data Bank.

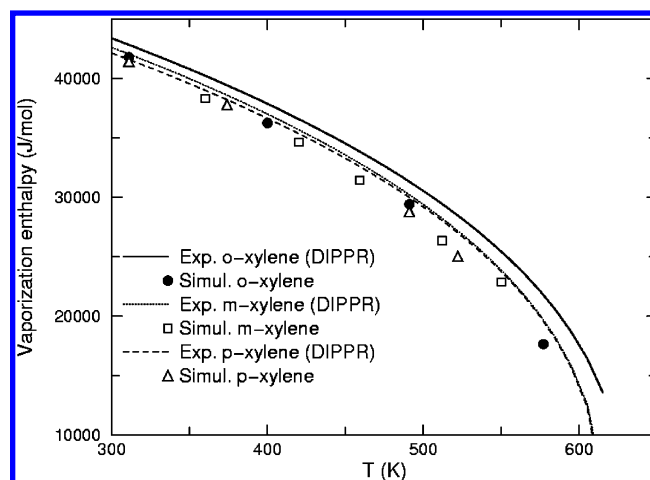


Figure 4. Vaporization enthalpy of xylene isomers computed with the new AUA potential. Comparison is given with the correlations of experimental data provided by the Dortmund Data Bank.

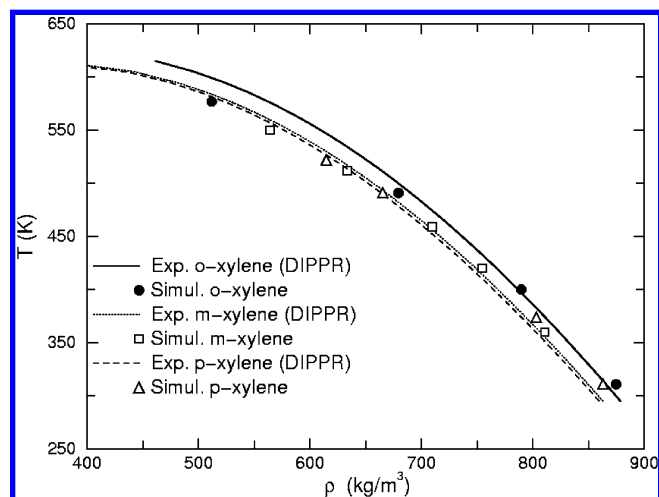


Figure 5. Saturated liquid density of xylene isomers computed with the new AUA potential. Comparison is given with the correlations of experimental data provided by the Dortmund Data Bank.

the saturation pressure are small as compared with the degree of variation of this property over the range of conditions investigated (more than 7 orders of magnitude).

TABLE 6: Equilibrium Properties of *n*-Propylbenzene Obtained by Simulation with Proposed AUA Potential As Compared with DIPPR Correlations of Experimental Measurements

T (K)	ρ (kg/m ³)				ΔH_{vap} (kJ/mol)			P^{sat} (kPa)		
	vapor	liquid								
	AUA	AUA	exp	% dev	AUA	exp	% dev	AUA	exp	% dev
300								0.68 ₁₂	0.52	30.8
321.43		849.6 _{2,5}	838.5	1.3	45.8 ₂	45.0	1.8	2.10 ₂₅	1.75	20.0
346.15		828.3 _{1,8}	816.5	1.4	44.3 ₂	43.6	1.7	7.8 _{1,2}	5.7	37.5
375		796.4 _{2,6}	789.8	0.8	42.2 ₂	41.9	0.8	22.5 _{2,5}	17.8	26.4
409.09		765.3 _{3,1}	756.8	1.1	40.3 ₂	39.7	1.4	74.5 ₁₀	53.6	38.9
450	6.7 ₅	724.0 _{3,1}	714.5	1.3	36.9 ₂	36.8	0.2	193 ₁₃	155.9	24.0
500	18.0 _{2,7}	664 ₅	657.0	1.0	31.8 ₄	32.7	−2.6	534 ₇₁	439	21.8
550	44 ₄	594 ₁₀	589.1	0.8	26.6 ₆	27.5	−3.4	1247 ₁₁₃	1006	23.9
600	99 ₁₆	483 ₂₁	497.9	−3.0	17 ₁	19.9	−13.6	2430 ₂₉₃	2010	20.9
avg absolute dev (%)				1.1 ^a						27.1

^a The 600 K point has been excluded.**TABLE 7: Equilibrium Properties of *n*-Hexylbenzene Obtained by Simulation with Proposed AUA Potential As Compared with DIPPR Correlations of Experimental Measurements**

T (K)	ρ (kg/m ³)				ΔH_{vap} (kJ/mol)			P^{sat} (kPa)		
	vapor	liquid								
	AUA	AUA	exp	% dev	AUA	exp	% dev	sim	exp	% dev
310.15		862.6	845.9	2.0	61.1	59.4	2.9	0.035	0.042	−17.7
330.66		846.0	830.8	1.8	59.5	58.0	2.5	0.18	0.16	15.1
354.07		827.5	813.1	1.8	57.6	56.4	2.1	0.60	0.57	5.1
381.06		804.4	792.2	1.5	55.4	54.4	1.7	2.8	2.1	34.4
412.49		778.8	767.0	1.5	53.1	52.0	2.0	8.7	7.8	10.4
449.58		743.7	735.7	1.1	49.9	49.0	1.9	36.7	29.0	26.5
494.00	3.9	698.2	695.6	0.4	45.8	45.0	1.8	95.6		
548.16	13.5	642.2	641.2	0.2	40.1	39.4	1.7	333		
615.65	43.1	550.7	558.4	1.6	30.7	30.5	0.7	1000		
avg absolute dev (%)				1.2						2.0

In Table 9, we indicate the normal boiling temperature, the critical temperature, and the critical density of the alkylbenzenes and styrene investigated. The benzene results¹⁹ are given to indicate the general trend for all aromatics investigated so far. The comparison with experimental data must be made with caution, as the heavier hydrocarbons that have been investigated are not sufficiently stable at high temperature to allow a direct measurement of their critical coordinates. This is the case of *n*-dodecylbenzene and also of *n*-hexylbenzene to a lesser extent. Similarly, the boiling temperature of *n*-dodecylbenzene is obtained by extrapolation. To restrict comparison to true experimental measurements, these points have not been considered when evaluating the average absolute deviations. The

average error is thus 1.5% on the normal boiling temperature, 2.2% on the critical temperature, and 3.3% on the critical density.

5. Discussion

The new AUA parameters obtained for the aromatic carbon may be compared first of all with the AUA parameters of the aromatic CH group calibrated on benzene or with the parameters of olefinic groups. The Lennard–Jones diameter (3.0648 Å) is slightly less than the aromatic CH group (3.2464 Å) and close to the 3.02 Å of the branched olefinic C group.¹⁷ This small difference is not surprising, as it is expected that these diameters should be representative of the thickness of the aromatic or polyaromatic sheets. The energetic parameter of the new C group (42.079 K) is much smaller than the 89.415 K of the aromatic CH group. This is not unexpected since the decrease of the energetic parameter with decreasing number of bonded hydrogens has been already noticed with branched alkanes¹⁵ and with olefins.¹⁷ However, the difference with the energetic parameter of the branched olefinic C group (61.9 K) cannot be explained simply. It is likely that for such hidden groups, the determination of optimal parameters is sensitive to a possible bias in the previous optimization of the other groups.

We also notice that the optimized set of parameters has favored the representation of the density and vaporization enthalpy at the expense of the saturation pressure. It is possible that a slightly different set of parameters would have been obtained if a larger weight had been given to the saturation pressure reference in the error criterion.

When considering all the tests performed on various alkylbenzenes, it may be stated that they have evidenced the same qualities and pitfalls as the reference molecule (i.e., *p*-xylene).

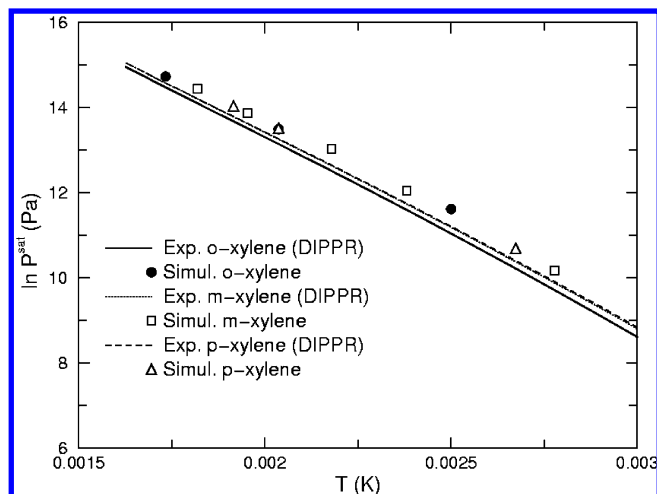


Figure 6. Vapor pressures of xylene isomers computed with the new AUA potential. Comparison is given with the correlations of experimental data provided by the Dortmund Data Bank.

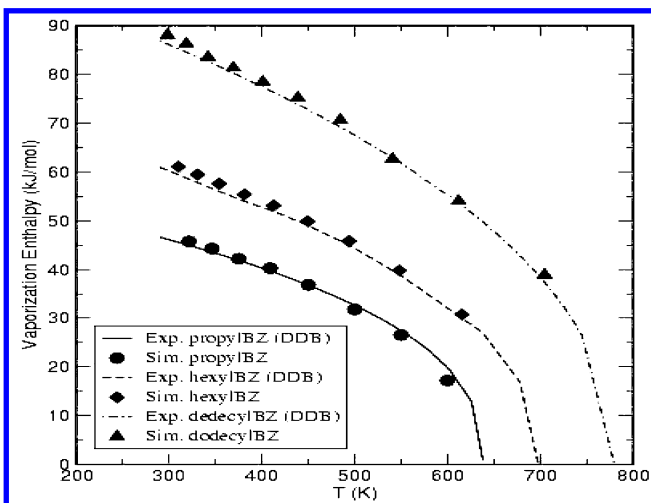
TABLE 8: Equilibrium Properties of *n*-Dodecylbenzene Obtained by Simulation with Proposed AUA Potential As Compared with DIPPR Correlations of Experimental Measurements

<i>T</i> (K)	ρ (kg/m ³)				ΔH_{vap} (kJ/mol)			P^{sat} (kPa)		
	vapor AUA	liquid		% dev	ΔH_{vap}		% dev	P^{sat}		% dev
		AUA	exp		AUA	exp		AUA	exp	
298.15		864.0 _{1.8}	852.2	1.4	88.1 _{0.4}	86.3	2.1	2.4×10^{-5} _{5.5 \times 10^{-6}}	2.3×10^{-5}	6.4
318.57		851.3 _{1.4}	838.2	1.6	86.3 _{0.4}	84.6	2.0	2.6×10^{-4} _{3.8 \times 10^{-5}}	2.0×10^{-4}	27.0
341.99		833.4 _{3.5}	821.8	1.4	83.5 _{0.8}	82.7	1.0	2.1×10^{-3} _{4.6 \times 10^{-4}}	1.7×10^{-3}	22.8
369.14		818.8 _{1.7}	802.6	2.0	81.4 _{0.4}	80.3	1.3	1.9×10^{-2} _{3.0 \times 10^{-3}}	1.4×10^{-2}	41.7
400.96		793.6 _{3.1}	779.5	1.8	78.5 _{1.0}	77.5	1.3	0.14 _{0.04}	0.10	38.8
438.79		766.5 _{2.5}	751.2	2.0	75.2 _{0.9}	73.9	1.8	1.1 _{0.1}	0.7	59.6
484.49		732.4 _{3.2}	715.7	2.3	70.7 _{0.7}	69.3	2.0	6.9 _{1.6}	4.4	56.1
540.83		678.7 _{3.5}	669.3	1.4	62.7 _{0.8}	63.0	−0.5	43.4 _{5.4}	25.2	72.4
611.99	9.4 _{1.6}	615.0 _{6.4}	604.3	1.8	54.0 _{1.2}	53.7	0.6	177 ₃₀	128	38.5
704.71	38.7 _{2.8}	498.7 _{8.0}	498.9	0.0	38.9 _{0.8}	37.4	3.9	710 ₄₄	589	20.5
avg absolute dev (%)				1.6						38.4

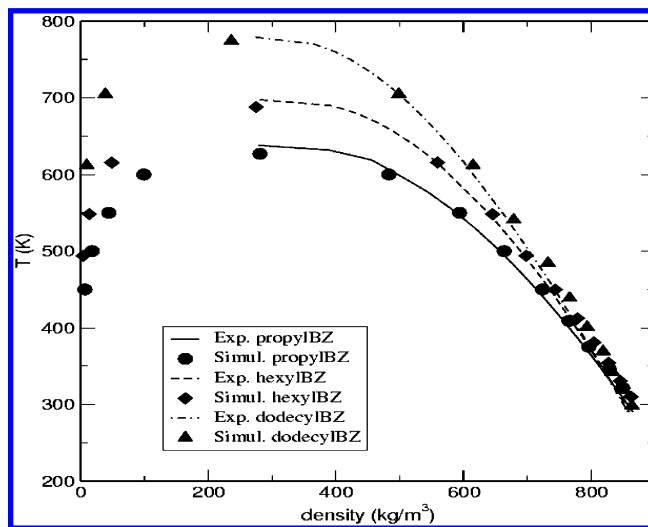
TABLE 9: Estimated Critical Temperature, Critical Density, and Normal Boiling Temperature of Alkylbenzenes Considered^a

	T_c (K)			ρ_c (kg/m ³)			T_b (K)		
	AUA	exp	% dev	AUA	exp	% dev	AUA	exp	% dev
benzene	558	562.1	−0.6	302	302	0.0	350	353.2	−0.9
toluene	580	594.0	−2.4	307	309	−0.7	376	383.8	−2.0
<i>o</i> -xylene	610	630.3	−3.2	311	289	7.5	403	417.1	−3.4
<i>m</i> -xylene	604	617.0	−2.1	287	280	2.5	402	412.3	−2.5
<i>p</i> -xylene	598	616.3	−3.0	303	281	7.9	402	411.2	−2.0
1,3,5-trimethylbenzene	622	637.4	−2.4	283	280	1.1	421	438	−3.9
styrene	629	636	−1.1	295	297	−0.7	415	418.2	−0.8
<i>n</i> -propylbenzene	627	638.2	−1.8	281	273	2.9	422	432.4	−2.4
<i>n</i> -hexylbenzene	688	698	−1.4*	275	274	−1.6	491	499.0	−1.4
<i>n</i> -dodecylbenzene	774	780	−0.7*	236	267	−11.6	584	600.0	−2.7*
avg absolute dev (%)			2.1						2.2

^a Computed values (AUA) are compared with experimental data (DIPPR Data Bank). Temperatures are expressed in K, and Density is in kg/m³. Deviations marked with an asterisk (*) have not been included when computing the average deviation, as the corresponding “experimental” information was based on large extrapolations.

**Figure 7.** Vaporization enthalpy of *n*-propylbenzene, *n*-hexylbenzene, and *n*-dodecylbenzene. Simulation results obtained with the new AUA potential are compared with the correlations of the Dortmund Data Bank.

They have similarly shown that a very good accuracy is obtained for liquid densities (Figures 2, 5, and 8) and vaporization enthalpies (Figures 1, 4, and 7). Vapor pressures are overestimated by approximately 30% on average (Tables 4–7). However, a satisfactory aspect of the proposed parameter set is that the errors on the vapor pressure of *n*-alkylbenzenes do not increase when much lower temperatures are considered (Figure 9). This good behavior of the vapor pressures may be attributed to the good prediction of vaporization enthalpy at low temperature, as this property controls the temperature dependence of vapor pressure. Before concluding about vapor pressure, it must

**Figure 8.** Vapor and liquid densities of *n*-propylbenzene, *n*-hexylbenzene, and *n*-dodecylbenzene. Simulation results obtained with the new AUA potential are compared with the correlations of the Dortmund Data Bank.

be recalled that this property is very sensitive to temperature. If we evaluate our predictions through the normal boiling temperature, the average deviation is only 1.5% (Table 9). From our perspective, this is a more meaningful test than critical properties for the compounds considered, as the critical point of heavy hydrocarbons is often impossible to measure because of the rapid thermal degradation at the high-temperature conditions of their critical points.

Among the compounds tested, the *n*-alkylbenzenes are better predicted than the dimethyl- and trimethylbenzenes. Indeed, the

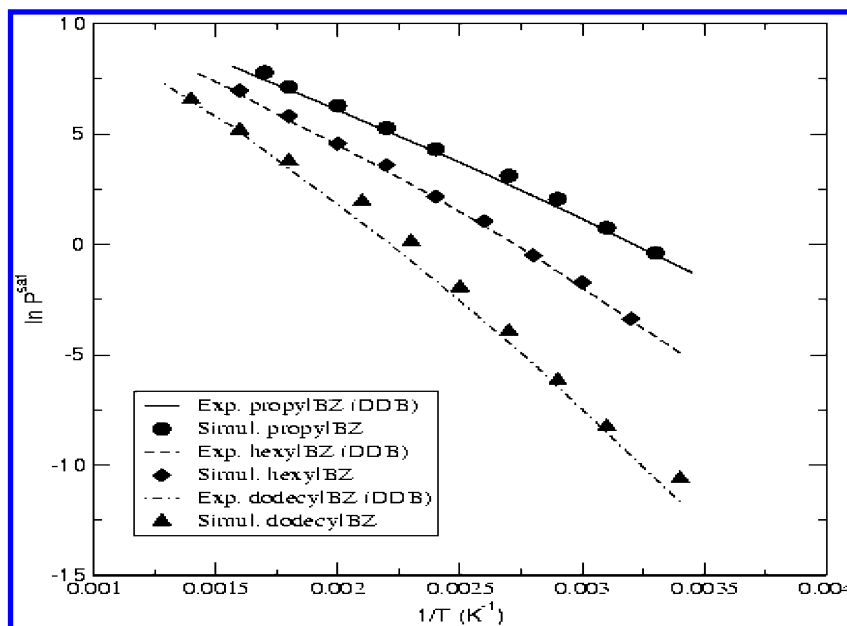


Figure 9. Saturated vapor pressure of *n*-propylbenzene, *n*-hexylbenzene, and *n*-dodecylbenzene. Simulation results obtained with the new AUA potential are compared with the correlations of the Dortmund Data Bank.

latter are subject to a more significant underestimation of the vaporization enthalpy at high temperature, a feature indicating the underestimation of their critical temperature (Figures 1 and 4).

An interesting issue is the prediction of property differences between isomers composed of the same groups. In our set, *o*-, *m*-, and *p*-xylene allow for such a comparison. Although small with respect to absolute deviations, the property differences between *o*-, *m*-, and *p*-xylene are of the same sign as indicated from experimental measurements (Tables 5 and 9). This observation is encouraging, but more accurate calculations and the investigation of other pairs are needed to evaluate the capacity of predicting differences between isomers.

The good results of these tests confirm the findings of Wick et al.⁹ that it is not necessary to consider electrostatic forces to predict the thermodynamic properties of aromatic hydrocarbons. It can be argued that neglecting electrostatic energy might be the reason systematic deviations are observed, such as the underestimation of vapor pressures. If this were true, we would expect that the molecules displaying significant dipole moments, like toluene or orthoxylene, would be poorly predicted while molecules such as paraxylene or 1,3,5-trimethylbenzene would be better predicted. This is not the case in our results.

6. Conclusion

The proposed parameter set for the C group of alkyl-substituted aromatics obtained from the optimization of *p*-xylene properties appear to provide good predictions for the C7–C18 alkylbenzenes and styrene investigated in the present study. Heats of vaporization, liquid densities, and normal boiling temperatures are predicted with an average accuracy of approximately 2%. These predictions confirm the good transferability of the AUA intermolecular potential. In particular, the benzene-based parameters for the aromatic CH group, the alkane-based CH, CH₂ and CH₃ alkyl groups, and the π alkene-based parameters for the CH and CH₂ vinyl groups have been used without modification and without introducing binary parameters to compute unlike interactions. This transferability is considered to be the result of the good physical sense of the potential parameters, which were shown to reproduce correctly

the liquid structure of benzene. The qualitative prediction of some property differences between xylene isomers is also a satisfactory feature of the model. However, the observation of systematic deviations on properties such as normal boiling temperatures suggests that it might be possible to refine the model in future work. Another perspective is the investigation of the properties of naphthenoaromatic and polyaromatic hydrocarbons, which will be considered in the next article of the present series.

Acknowledgment. This work has been supported by the Ministerio de Ciencia y Tecnología of the Spanish Government (PPQ2000-2888E and PPQ2001-0671) and the Generalitat de Catalunya (2000ACI-13, 2001ACI-39, and ACI2002-37). R.O.C.-C. would like to thank the University Rovira i Virgili for financial support. M.G.A. thanks the company Total for financial support, and the authors personally thank François Montel for his interest in the work and fruitful discussions.

References and Notes

- (1) Panagiotopoulos, A. Z. *Mol. Phys.* **1987**, *61*, 813–826.
- (2) Smit, B.; Karaborni, S.; Siepmann, J. I. *J. Chem. Phys.* **1995**, *102*, 2126.
- (3) Martin, M. G.; Siepmann, J. I. *J. Phys. Chem. B* **1998**, *102*, 2569.
- (4) Nath, S. A.; Escobedo, F. A.; de Pablo, J. J. *J. Chem. Phys.* **1998**, *108*, 9905.
- (5) Lopez-Rodriguez, A.; Vega, C.; Freire, J. J. *J. Chem. Phys.* **1999**, *111*, 438.
- (6) Martin, M. G.; Siepmann, J. I. *J. Phys. Chem. B* **1999**, *103*, 4508.
- (7) Nath, S. K.; de Pablo, J. J. *Mol. Phys.* **2000**, *98*, 231–238.
- (8) Spyriouni, T.; Economou, I. G.; Theodorou, D. N. *J. Am. Chem. Soc.* **1999**, *121*, 3407–3413.
- (9) Wick, C. D.; Martin, M. G.; Siepmann, J. I. *J. Phys. Chem. B* **2000**, *104*, 8008.
- (10) Nath, S. K.; Banaszak, B. J.; de Pablo, J. J. *J. Chem. Phys.* **2001**, *114*, 3612.
- (11) Errington, J. R.; Panagiotopoulos, A. Z. *J. Phys. Chem. B* **1999**, *103*, 6314.
- (12) Errington, J. R.; Panagiotopoulos, A. Z. *J. Chem. Phys.* **1999**, *111*, 9731.
- (13) Chen, B.; Siepmann, J. I. *J. Phys. Chem.* **1999**, *103*, 5370–5379.
- (14) Ungerer, P.; Beauvais, C.; Delhomelle, J.; Boutin, A.; Rousseau, B.; Fuchs, A. H. *J. Chem. Phys.* **2000**, *112*, 5499–5510.
- (15) Bourasseau, E.; Ungerer, P.; Boutin, A.; Fuchs, A. H. *Mol. Simul.* **2002**, *28*, 317–336.

- (16) Bourasseau, E.; Ungerer, P.; Boutin, A. *J. Phys. Chem. B* **2002**, *106*, 5483.
- (17) Bourasseau, E.; Haboudou, M.; Boutin, A.; Fuchs, A. H.; Ungerer, P. *J. Chem. Phys.* **2003**, *118*, 3020.
- (18) Friedrich, A.; Lustig, R. *J. Mol. Liq.* **2002**, 98–99, 241.
- (19) Contreras-Camacho, R. O.; Ungerer, P.; Boutin, A.; Mackie, A. D. *J. Phys. Chem. B* **2004**, *108*, 14109.
- (20) Toxvaerd, S. *J. Chem. Phys.* **1997**, *107*, 5197.
- (21) Evans, D. J.; Watts, R. O. *Mol. Phys.* **1976**, *32*, 93.
- (22) Jorgensen, W. L.; Severance, D. L. *J. Am. Chem. Soc.* **1990**, *112*, 4768.
- (23) Jorgensen, W. L.; Laird, E. R.; Nguyen, T. B.; Tirado-Rives, J. *J. Comput. Chem.* **1993**, *14*, 206–215.
- (24) Allen, M. P.; Tildesley, D. J. *Computer Simulation of Liquids*; Oxford Science Publications: Oxford, 1987.
- (25) Dodd, L. R.; Boone, T. D.; Theodorou, D. N. *Mol. Phys.* **1993**, *78*, 961–996.
- (26) Kofke, D. A. *J. Chem. Phys.* **1993**, *98*, 4149.
- (27) Lide, D. R. *Handbook of Chemistry and Physics*; CRC Press: Boca Raton, FL, 1992.
- (28) Jorgensen, W. L.; Madura, J. D.; Swenson, C. J. *J. Am. Chem. Soc.* **1984**, *106*, 6638.
- (29) Mokbel, I.; Rauzy, E.; Meille, J. P.; Jose, J. *Fluid Phase Equilib.* **1998**, *147*, 271.